Research Article | Vol. 33, No. 15 / 28 Jul 2025 / Optics Express 31722
Optics EXPRESS

# Observation of spectrally continuous resonance enhancement by mode coalescence

Nitzan Shani,[1] Amit Kumar Shakya,[1] Fan Cheng,[1] Vladimir Shuvayev,[2] Lev Deych,[3] and Tal Carmon[1,*]

[1]School of Electrical Engineering, Tel Aviv University, Tel Aviv 6997801, Israel
[2]Physics Department, Queens College of CUNY, Flushing, Queens, New York 11367, USA
[3]The Graduate Center of CUNY, New York, New York 10016, USA
[*]total@tauex.tau.ac.il

**Abstract:** Microcavities rarely operate in a broadband regime and are, therefore, limited in their ability to resonantly enhance broadband light-matter interactions. Here, we present what is believed to be the first experimental demonstration of several overlapping spectrally continuous optical resonances. We rely on sufficiently long cylinders here, making the mode's axial quantum numbers turn from a discrete set into a continuous one. Except for potential perfect absorbers of white light and bright white microemitters, other waves in nature (e.g., sound, matter waves, and quantum probability densities) might similarly support perfect absorption of earthquakes, energy harnessing from sea waves, and fundamental studies in wave-matter interaction.



## 1. Introduction

Level crossing suggests certainty at its location; for example, in the energy-momentum space. Generally speaking, this certainty benefits measurements in fields ranging from fine-structure spectroscopy [1–3] and quantum two-state evolution [4–7] to graphene behavior [8] and sensing [9–22]. Crossings [1–26] were reported to be exceptional [9–22], avoided [25], simple [25,26], or of the Landau level [5,23–8] type [Fig. 1(a)-(d)]. In the case of resonators with discrete spectra, frequency degeneracy results from crossing between two levels [1–26], which is achieved by tuning a parameter, such as the ratio between the major and minor radii of a toroid [24]. When the cavity is an open resonator, with gain and loss involved, full degeneracy would require finding an exceptional point where both the real and imaginary parts of two complex eigenvalues coincide [9–22].

The situation is different in waveguides, where modes are characterized not only by discrete indices (e.g., radial and azimuthal in cylindrical waveguides) but also by a continuous axial wavevector parameter, $k_z$ (Fig. 1, e-i). This continuous axial wave vector relates to the nature of waveguides, among them optical fibers, which can carry all colors of light. Interestingly, this rule also applies to single-mode fibers where the longitudinal mode can have a variety of colors. However, these waveguide modes do not exhibit a resonance enhancement, as is typical in cavities with discrete spectra. In other words, waveguides trade off spectral continuity for resonance enhancement. Can we hold the stick from both ends and combine resonance enhancement with spectral continuity? Our simple answer is yes.

## 2. Theoretical framework

In detail, we overcome the seeming contradiction between the resonance enhancement and the discrete-frequency operation. This is achieved by benefiting from whispering gallery modes in cylindrical waveguides [27–29] (e.g., with different azimuthal numbers) that have a continuous longitudinal index ($k_z$), which implies spectral continuity and white-light compatibility. This modal configuration results in unique interference patterns, that evolve continuously along a wide

#561188 https://doi.org/10.1364/OE.561188
Journal © 2025 Received 5 Mar 2025; revised 8 May 2025; accepted 6 Jun 2025; published 21 Jul 2025

Optics EXPRESS

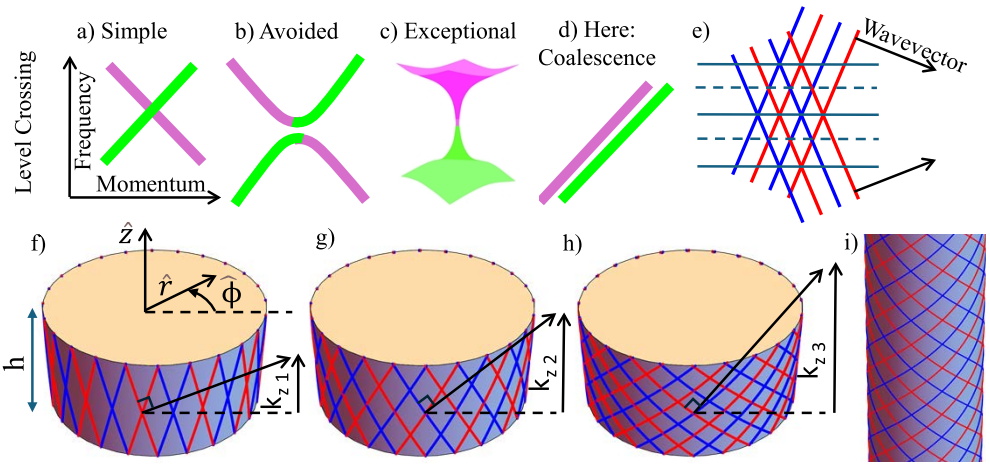


**Fig. 1.** (a-c) Level Crossing state of the art and d) level coalescence here. e) Plane-wave interference is dark along lines where field maximum meets field minimum (blue-red intersections), as marked by grey dashed lines, and light along the other junctions, as marked by a grey solid line. A finite disk resonator (f-h) contains azimuthally propagating waves that similarly interfere while the solid-phase boundary, at the cylinder's top and bottom faces, forces one (f), two (g), three (h), or other integer number of maxima along the axial direction. Differently, (i) longer cylinders, here, permit a continuous set of axial wavevectors spanning broad spectral bands, $\{k_{z\beta}\}$

spectral band, which we film here for the first time [Visualization 1]. In fact, using high-order whispering-gallery modes in axially symmetrical cylinders [27–29], we demonstrate simultaneous excitation of several frequency-degenerate modes that also continuously cover a broad range of frequencies. We film movies of these emerging interference patterns using a fluorescent spatial mode mapping technique while simultaneously monitoring spectral transmission. Combining resonance enhancement with spectral continuity can be utilized in fields such as compact CW supercontinuum generation or broadband perfect absorbers [30]. Similarly, all waves in nature, among them quantum probabilities and sound, can be broadband resonantly enhanced to facilitate perfect absorption [30] of earthquakes or energy harnessing of sea waves.

Modes of cylindrical waveguides are naturally characterized by two discrete and one continuous quantum numbers. This is in contrast with resonators that have only discrete quantum numbers. Relatedly, higher cavity finesse (or optical quality divided by mode volume, Q/V) suggests that resonances are narrower and farther apart. The cavity goodness of fit parameter, Q/V, that scales as the Purcell factor [31], was therefore thought of as inherently restricting continuous operation at the spectral domain. Can we compromise, to some extent, on Q/V to combine a continuous frequency spectrum, like waveguides, with resonance enhancement by cavities? Assuming a sufficiently long cylinder with modes at small propagation constants k characterized by the dispersion law [32]:

$$\omega = \sqrt{\omega_c^2 + \alpha^2 k^2}, \tag{1}$$

where $\omega_c$ is a cutoff frequency of the mode and $\alpha$ is the dispersion parameter arising upon expansion of the dispersion law of the mode in the powers of the wavenumbers. The exact expression for this parameter in terms of the parameters of the cylinder is not important since we only use Eq. (1) to demonstrate the general relationship between the dispersion properties of the modes and the Purcell factor. The Purcell factor is defined as a ratio of the density of state of an optical structure and that of the free propagating light. Using Eq. (1) it is easy to derive that the

Optics EXPRESS

$P(\omega)$ or these modes is

$$P(\omega) = 2\omega S / \left( c^3 \sum_j \alpha_j \sqrt{\omega^2 - \omega_{jc}^2} \right), \tag{2}$$

where we took into account that at any given frequency there might be several different modes contributing to the total number of states. Subindex j enumerates such modes, and S is the cross-sectional area of the cylinder, and c is the speed of light. These modes are characterized by azimuthal index M, reflecting the axial symmetry of the cylinder, and the radial index defining their behavior in the radial direction (single index j in the above equation incorporates both axial and radial indices). High-order modes with frequencies close to the corresponding cutoff frequency are characterized by small propagation constants and are very sensitive to small variations of the radius of the waveguide [27–29]. As shown in Ref. ( [28]) these modes can be localized between two random minuscule narrowing of the waveguide, resulting in characteristic standing wave intensity distributions and strong resonant enhancement. With increasing frequency, the modes delocalize, and several modes with the same frequency but different propagation constants can be excited simultaneously, interfering to result in a unique intensity distribution.

To qualitatively give an insight into the spectral continuity of cylinder modes and their overlapping, we start from the simple case of interference between plane waves [Fig. 1(e)]. Two plane waves, tilted one with respect to the other, generate a periodic pattern of uniformly spread maxima, or bright fringes [Fig. 1(e), gray line]. The larger the angle between these beams, the closer the distance between the interference fringes. In this regard, cylinder modes have maxima forming bright rings spreading along the axial direction, which can be similarly attributed to the interference between two helical waves, each with a different tilt. When the cylinder is short, and similar to a disk, dark regions are forced on its top and bottom faces [33] [Fig. 1(f-h)]. These dark circular fringes are associated with interference between field maxima [Fig. 1(f-h), red] and field minima [Fig. 1(f-h), blue]. That is, the disk's axial dimension spans a discrete set of axial resonances with i = 1, 2, 3, or more axial maxima. Again, this integer number relates to the disk's upper and lower solid-phase boundaries, implying dark regions at its top and bottom faces. In this formalism, the corresponding axial wavevectors are

$$k_{z\,i} = \pi n i / h, \tag{3}$$

where i is an integer index (i = 1,2,3. . . ) that numbers the elements of this set (i represents the number of maxima along the axial z axis), h is the height of the disk, and n is the effective refractive index. The first wavevector, $k_{z\,1}$, corresponds to a mode with one maximum along the axial direction [Fig. 1(f)], $k_{z\,2}$ corresponds to two maxima [Fig. 1(g)], and so on [Fig. 1(h)]. Relevant to our experiment, when the cylinder is long enough, $k_z$ turns from a discrete set, $\{k_{z\,1},\ k_{z\,2} \ldots . k_{z\,i}\}$, where i is an integer, into a continuous set $\{k_{z\,\beta}\}$, where the subscript $\beta$ is a continuously varying index [Fig. 1(e)]. In this long enough cylinder, the mode is axially confined by slight radius variations, as explained in Refs. [27,28,29]. Such modes were analyzed using a tapered fiber probe [28], used for measuring nanoscale variation in the cylinder radius [29], and to support light delays [27].

Our system combines resonator and fiber properties. This is because, similar to fibers that can carry all colors, its spectrum is continuous. And like an optical cavity, its modes are confined to a limited volume in space and resonantly enhanced, though with some compromise in coupling efficiency.

## 3. Experimental setup

Here, we spatially and spectrally map cylinder modes by filming movies that show, for the first time, coalesced modes that exhibit a 3D structure that continuously evolves while we scan the input wavelength. Furthermore, we measure that a few of the continuous cylinder modes

Optics EXPRESS

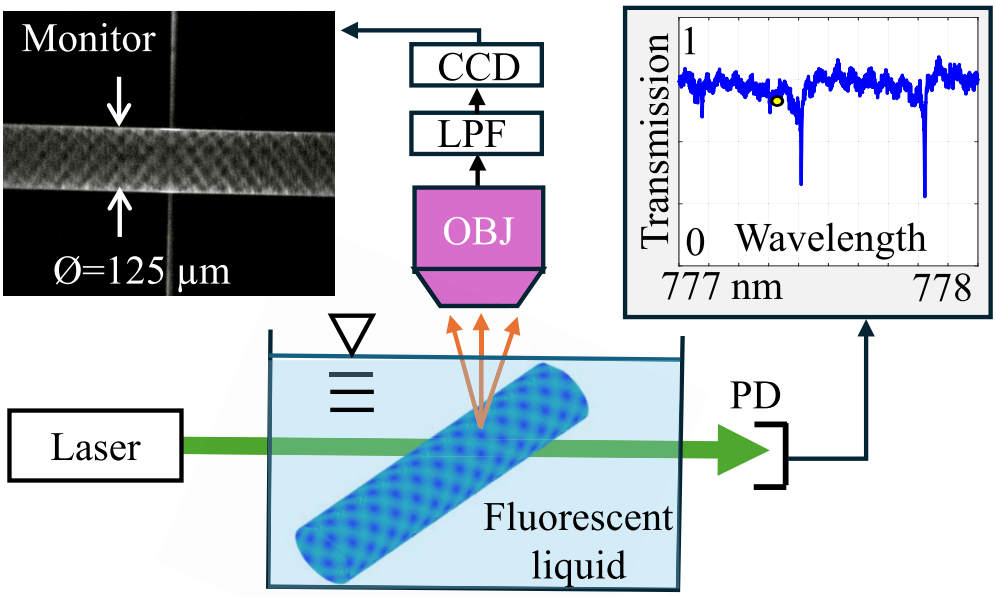


**Fig. 2.** Experimental setup: We couple light via a tapered fiber to excite the cylinder modes. We then scan the input wavelength while filming the modes (Visualization 1), using a fluorescent mode mapping technique, while simultaneously monitoring the spectral transmission using a photodiode [PD]. Altogether, this mapping provides a movie of the 3D structure of the mode evolution, together with the spectral transmission. LPF: long pass filter, OBJ: objective. Green: Fiber with tapering near the cylinder region. Blue: the dielectric cylinder with an interference pattern in the region where the optical resonances evanescently extend to the fluorescent liquid.

can coexist, as evidenced by their interference pattern. Most importantly, we observe several continuous resonances co-spreading a spectral continuum, making it almost impossible to find a wavelength without resonance.

Figure 3 shows three panels, with the rightmost panel illustrating a mode with a single bright circumferential ring, indicating an axial wavevector near zero. As the pump wavelength decreases, the axial component kz increases, leading to more concentric rings and stronger axial modulation. Notably, the central panel exhibits maximum delocalization, consistent with modes above the cutoff. The mode labeled M = 745M = 745M = 745 corresponds to the azimuthal quantum number and was chosen based on COMSOL simulations to ensure efficient coupling.

Our experimental setup [Fig. 2] includes light from a tunable laser at a wavelength near 780 nm, which we coupled to circumferentially circulate in the 3.5 cm-long dielectric cylinder (Corning SMF-28e fiber) using a tapered fiber [31] with a minimum waist diameter of 1 μm tapering gradient of ∼1/20. The cylinder is inserted through a gently placed hollow pipette, with ∼8 cm of it remaining inside the pipette and ∼3.5 cm submerged in the fluorescent liquid. The cylinder light containing region is typically 5 mm long, This configuration securely holds the fiber in place without introducing significant loss. The tapered fiber and the cylinder are positioned at a 90° angle, allowing efficient coupling to whispering-gallery modes. We control the position of the taper, relative to the cylinder, using a nano-cube. We use a photodiode connected through the other side of the taper to measure the spectral transmission through the cylinder. While we scan the input wavelength, we film the 3D image of its evolving structure. These movies are taken by submerging the cylinder in a fluorescent liquid (water with 3 $\mu$mol/L ADS780WS by American Source Dye Inc.) to convert part of the resonance mode to spontaneous emission at

Optics EXPRESS

longer wavelengths. A long pass filter is combined with a microscope to take micrographs of the fluorescent emission marking mode structure. Fluorescent light benefits imaging here by emitting incoherently and in all directions, facilitating better resolution in combination with an increased amount of light penetrating through the objective. Furthermore, the cylinder modes are

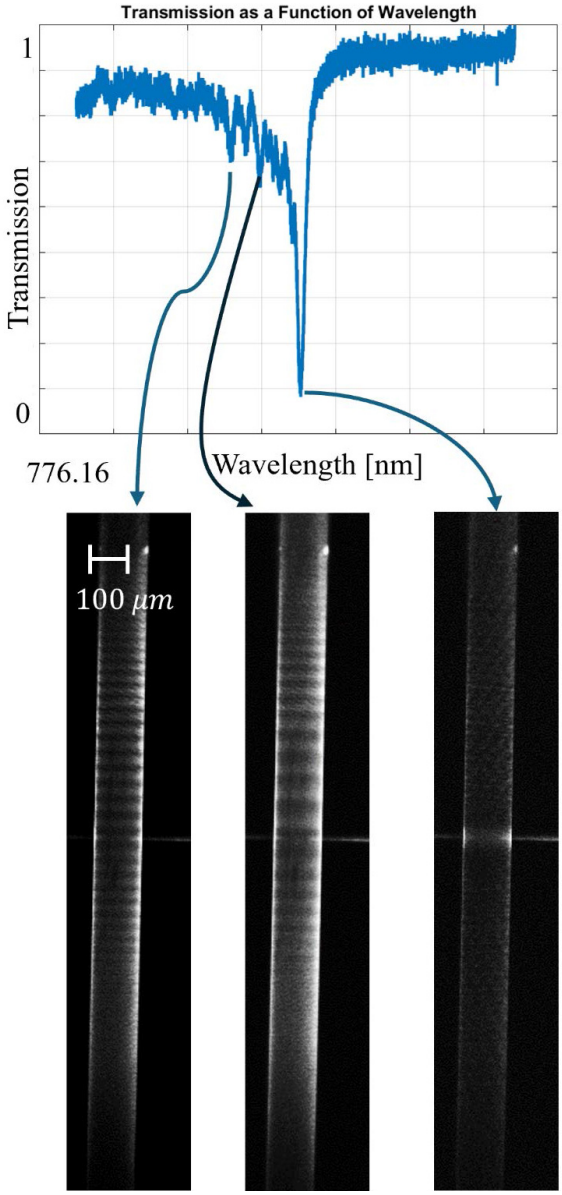


**Fig. 3.** Experimental results: fundamental mode with azimuthal number M = 745 (supported by theoretical simulations), exhibiting a single-ring structure when its axial wavevector is zero ($K_z = 0$) as shown on the right panel. As pump wavelengths goes shorter, the axial wavevector, $K_z$ gets larger than the cutoff for the mode with M = 745 – resulting in an interference pattern with an increasing number of fringes, each of them is ring shaped.

Optics EXPRESS

evanescently extending into a short distance (~10 nm) within the fluorescent liquid, benefiting sharper images given the small depth of focus typical of microscopes.

## 4. Results

Our experimental results include the first photographs of cylinder modes [Fig. 3 and supplementary movie 1] and show that the cylinder mode continuously develops from having a single circumferential ring to many concentric rings, multiplying as the input wavelength turns shorter. Depending on the wavelength scan direction, we can control the ring pattern to shrink or expand. Such control over the number of rings and their location might be useful in the controlled trapping of nanoparticles [34,35]. We observe that the dielectric cylinder modes are continuously changing their spatial distribution during the wavelength scan. As a result, the external source coupling coefficient changes with the overlap between the taper and cylinder modes. As for the transmission, it falls from a nearly critical coupling when the axial mode order is small and has a large overlap with the tapered fiber mode. Importantly, the modes are photographed at any location along the entire spectrum, whereas high-order resonances are under-coupled as indicated by a higher transmission. Such an under-coupling can benefit laser modes, as explained in [36,37]. The theoretical limit on the Q-factor of a cylindrical microresonator [28] is 2.542 times less than that of a spheroidal microresonator fabricated from the same material and having the same radius, meaning that $10^8$ Qs are possible in cylinders. Importantly, linewidth such as in Fig. 3 does not stand for the quality factor but for a spectrally continuous mode ensemble. Such

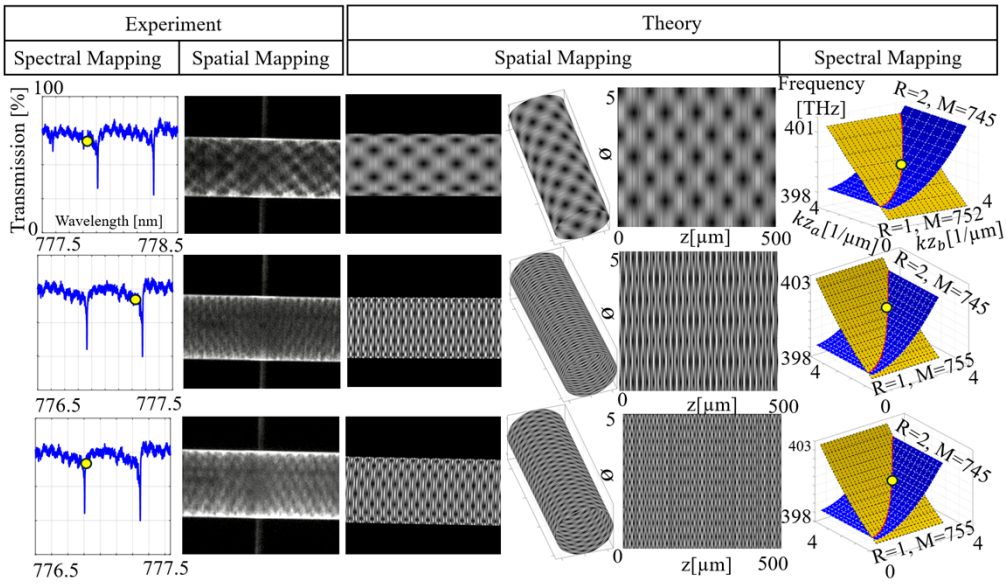


**Fig. 4.** Mode coalescence. (Left) Experimental results: the spectral transmission of the cylinder, where the yellow point represents the wavelength at which the spatial-mapping micrograph was taken. (Right) Theory: Spatial interference between two modes next to their spectral mapping at the energy-momentum space. M: the azimuthal order of the mode. R: the radial order of the modes. $k_{z,a}$ and $k_{z,b}$ : the axial momenta of the two coalesced modes. Red line: representing the frequency through which a continuous interference appears, and two modes coalesce and coexist (Visualization 1). Yellow point: the energy-momentum place where the experimental frame from the movie was taken.

Optics EXPRESS

high-Qs of a continuous spectrum were demonstrated in resonators of larger sizes [38] where higher-order transverse modes cover the free spectral range.

Unlike in Fig. 3, where one mode dominates, Fig. 4 presents the very common situation of having two spectrally continuous modes, which is included in Movie 1. The two modes are indicated by an azimuthal interference pattern between them. For example, two modes having azimuthal indices $M_1 = 745$ and $M_2 = 752$, representing the number of wavelengths that are resonating along their circumference, make an interference pattern with $M_2$ - $M_1 = 7$ circumferential maxima [Fig. 4, top row]. Importantly, such orthogonal mode pairs (e.g., $M_1 = 745$ and $M_2 = 752$) are excited at the same laser frequency. While such different M modes will typically have different resonance frequencies that are separated by a spectral gap; here, the continuously changing axial order of the modes, and a different radial index, can compensate for that gap. In detail, and as seen [Fig. 4, right column, red line, and Visualization 1, the continuity of the axial indices, $\beta$, results in a supercontinuum coalescence where the interferogram continuously exists and spatially evolves due to the variation in the axial momenta of the interfering modes [Fig. 4 right column]. These bands, where modes are continuous, differ from those observed in finite resonators, where level crossing represents a spectrally singular [24–26] event. Of course, when the wavelength is stationary, the interference pattern is standing too. Such interference is generally referred to as a stopped light [25], representing its zero phase velocity and a stationary character.

We also measure coalescence between 3 modes, as evidenced by an interference pattern with 7 and 10 circumferential maxima [Fig. 5]. As one can see in Fig. 5(a), in some regions the

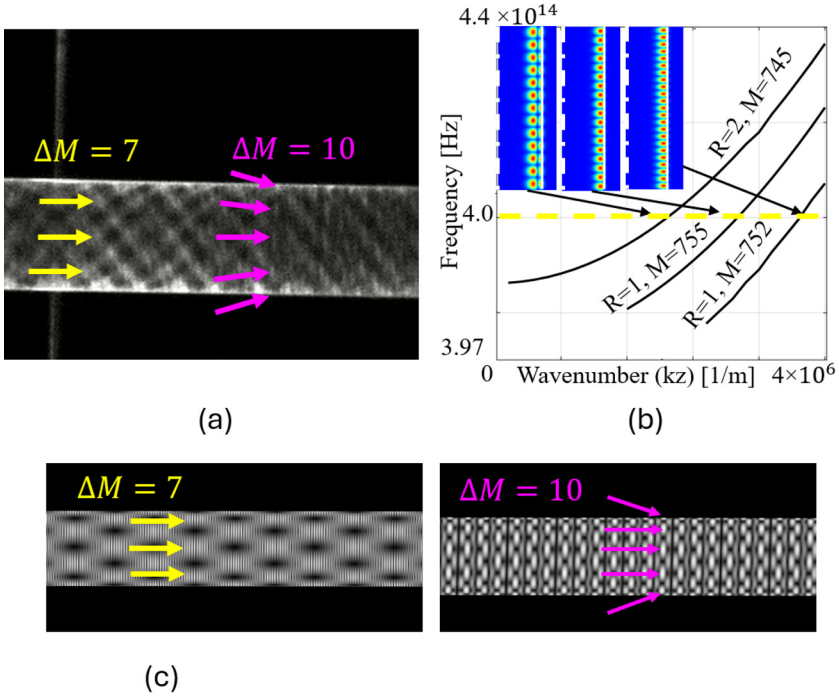


**Fig. 5.** (a) Experimental observation of 3-mode coalescence as indicated by a micrograph where 7 and 10 circumferential maxima are seen. (b) spectral mapping of the energy-momentum space showing the 3-mode on the left can coexist in the cylinder for a single pump frequency value. (c) Theoretical interference patterns calculated for the mode pairs from (b) with $\Delta M = 7$ and $\Delta M = 10$, corresponding to the experimental features observed in (a).

Optics EXPRESS

mode pair with $\Delta M = 7$ dominates and in other regions, the mode with $\Delta M = 10$ dominates; we accordingly theoretically calculated the interference pattern for these two cases [Fig. 5.c], when a pair of mode dominates. Note that we expect to see half of interference pattern when side viewing it (e.g., 5 fringes for the $\Delta M = 10$)"

## 5. Conclusions

In conclusion, we demonstrate that a dielectric cylinder supports the coalescence of its resonances to exhibit a continuous spectrum. Regarding perfect absorption, while our resonator benefits from a continuous spectrum, many modes operate in the under-coupled regime so that their acceptance by the cavity is limited. This is due to the spectral change in mode shape. Although challenging, overcoming this limitation will allow perfect absorption of white light. Adding optical gain to such a cylinder will support frequency supercontinuum micro-emitters. This is different from current supercontinuum technology, which is based on large photonic-crystal fiber-based emitters that operate in short pulses (and not continuously in time, as proposed here). General to all waves in nature, similar resonators might permit resonantly enhancing or perfectly absorbing [30] spectrally broad waves ranging from sound (in the form of white noise or shock waves) to quantum probability densities of electrons, thereby extending resonantly enhanced wave-matter interaction to broad bands. Furthermore, our spectrally continuous resonance enhancement might benefit applications ranging from perfectly absorbing unwanted waves, such as sound and earthquakes, to harnessing energy from abundant waves, among them sea waves.

**Funding.** United States-Israel Binational Science Foundation (2020683); Israel Science Foundation (537/20).

**Acknowledgment.** N.S. and F.C. performed the experiments. V.S. performed the theoretical analysis. A.S. performed the analytical analysis. L.D. supervised the work. T.C. supervised all aspects of the work.

**Disclosures.** The authors declare no conflicts of interest.

**Data availability.** Data underlying the results presented in this paper are not publicly available at this time but may be obtained from the authors upon reasonable request.

## References

1. F. D. Colegrove, P. A. Franken, R. R. Lewis, *et al.*, "Novel Method of Spectroscopy With Applications to Precision Fine Structure Measurements," Phys. Rev. Lett. **3**(9), 420–422 (1959).
2. K. Sowmya, K. N. Nagendra, M. Sampoorna, *et al.*, "Polarized Light Scattering with the Paschen–Back Effect, Level-Crossing of Fine Structure States, and Partial Frequency Redistribution," Astrophys. J. **793**(2), 71 (2014).
3. A. Windberger, J. R. Crespo López-Urrutia, H. Bekker, *et al.*, "Identification of the Predicted 5 s – 4 f Level Crossing Optical Lines with Applications to Metrology and Searches for the Variation of Fundamental Constants," Phys. Rev. Lett. **114**(15), 150801 (2015).
4. I. Das, X. Lu, J. Herzog-Arbeitman, *et al.*, "Symmetry-broken Chern insulators and Rashba-like Landau-level crossings in magic-angle bilayer graphene," Nat. Phys. **17**(6), 710–714 (2021).
5. E. Gornik, G. Strasser, and K. Unterrainer, "Landau level laser," Nat. Photonics **15**(12), 875–883 (2021).
6. V. Subramanyan, S. S. Hegde, S. Vishveshwara, *et al.*, "Physics of the Inverted Harmonic Oscillator: From the lowest Landau level to event horizons," Ann. Phys. **435**, 168470 (2021).
7. J. Wang, J. Cano, A. J. Millis, *et al.*, "Exact Landau Level Description of Geometry and Interaction in a Flatband," Phys. Rev. Lett. **127**(24), 246403 (2021).
8. E. McCann and V. I. Fal'ko, "Landau-level degeneracy and quantum Hall effect in a graphite bilayer," Phys. Rev. Lett. **96**(8), 086805 (2006).
9. W. D. Heiss, "Repulsion of resonance states and exceptional points," Phys. Rev. E **61**(1), 929–932 (2000).
10. C. Dembowski, H. D. Gräf, H. L. Harney, *et al.*, "Experimental observation of the topological structure of exceptional points," Phys. Rev. Lett. **86**(5), 787–790 (2001).
11. M. Liertzer, L. Ge, A. Cerjan, *et al.*, "Pump-induced exceptional points in lasers," Phys. Rev. Lett. **108**(17), 173901 (2012).
12. J. Wiersig, "Enhancing the sensitivity of frequency and energy splitting setection by using exceptional points: application to microcavity sensors for single-particle detection," Phys. Rev. Lett. **112**(20), 203901 (2014).
13. N. Zhang, S. Liu, K. Wang, *et al.*, "Single nanoparticle detection using far-field emission of photonic molecule around the exceptional point," Sci. Rep. **5**(1), 11912 (2015).
14. B. Peng, ŞK Özdemir, M. Liertzer, *et al.*, "Chiral modes and directional lasing at exceptional points," Proc. Natl. Acad. Sci. **113**(25), 6845–6850 (2016).

Optics EXPRESS


15. H. Xu, D. Mason, L. Jiang, *et al.*, "Topological energy transfer in an optomechanical system with exceptional points," (2016).
16. W. Chen, Ş Kaya Özdemir, G. Zhao, *et al.*, "Exceptional points enhance sensing in an optical microcavity," Nature **548**(7666), 192–196 (2017).
17. H. Hodaei, A. U. Hassan, S. Wittek, *et al.*, "Enhanced sensitivity at higher-order exceptional points," Nature **548**(7666), 187–191 (2017).
18. M.-A. Miri and A. Alù, "Exceptional points in optics and photonics," Science **363**(6422), eaar7709 (2019).
19. Y.-H. Lai, Y.-K. Lu, M.-G. Suh, *et al.*, "Enhanced sensitivity operation of an optical gyroscope near an exceptional point," (2019).
20. K. Özdemir, S. Rotter, F. Nori, *et al.*, "Parity–time symmetry and exceptional points in photonics," Nat. Mater. **18**(8), 783–798 (2019).
21. Y. H. Lai, Y. K. Lu, M. G. Suh, *et al.*, "Observation of the exceptional-point-enhanced Sagnac effect," Nature **576**(7785), 65–69 (2019).
22. M. P. Hokmabadi, A. Schumer, D. N. Christodoulides, *et al.*, "Non-Hermitian ring laser gyroscopes with enhanced Sagnac sensitivity," Nature **576**(7785), 70–74 (2019).
23. B. I. Halperin, P. A. Lee, and N. Read, "Theory of the half-filled Landau level," Phys. Rev. B **47**(12), 7312–7343 (1993).
24. T. Carmon, H. G. L. Schwefel, L. Yang, *et al.*, "Static envelope patterns in composite resonances generated by level crossing in optical toroidal microcavities," Phys. Rev. Lett. **100**(10), 103905 (2008).
25. A. A. Savchenkov, A. B. Matsko, V. S. Ilchenko, *et al.*, "Direct observation of stopped light in a whispering-gallery-mode microresonator," Phys. Rev. A **76**(2), 023816 (2007).
26. S. T. Attar, V. Shuvayev, L. Deych, *et al.*, "Level-crossing and modal structure in microdroplet resonators," Opt. Express **24**(12), 13134 (2016).
27. M. Sumetsky, "Delay of Light in an Optical Bottle Resonator with Nanoscale Radius Variation: Dispersionless, Broadband, and Low Loss," Phys. Rev. Lett. **111**(16), 163901 (2013).
28. M. Sumetsky, "Mode localization and the Q-factor of a cylindrical microresonator," Opt. Lett. **35**(14), 2385–2387 (2010).
29. M. Sumetsky, "Theory of SNAP devices: basic equations and comparison with the experiment," Opt. Express **20**(20), 22537–22554 (2012).
30. Y. Slobodkin, G. Weinberg, H. Hörner, *et al.*, "Massively degenerate coherent perfect absorber for arbitrary wavefronts," Science **377**(6609), 995–998 (2022).
31. C.-H. Chien, S.-H. Wu, T. H. B. Ngo, *et al.*, "Interplay of Purcell Effect, Stimulated Emission, and Leaky Modes in the Photoluminescence Spectra of Microsphere Cavities," Phys. Rev. Appl. **11**(5), 051001 (2019).
32. Bahaa E.A Saleh and Malvin Carl Teich, in *Fundamentals of Photonics*, 3rd ed. (Wiley, 2019), 1, p. Chap. 9, p. 360.
33. L. Yu, M. Cheng, K. Wang, *et al.*, "Analysis of giant forward Brillouin gain enhancement in double-disk microcavities by tailoring optical forces," Opt. Laser Technol. **141**, 107173 (2021).
34. S. Arnold, D. Keng, S. I. Shopova, *et al.*, "Whispering gallery mode carousel–a photonic mechanism for enhanced nanoparticle detection in biosensing," Opt. Express **17**(8), 6230–6238 (2009).
35. G. Tkachenko, V. G. Truong, C. L. Esporlas, *et al.*, "Evanescent field trapping and propulsion of Janus particles along optical nanofibers," Nat. Commun. **14**(1), 1691 (2023).
36. G. Bahl, J. Zehnpfennig, M. Tomes, *et al.*, "Stimulated optomechanical excitation of surface acoustic waves in a microdevice," Nat. Commun. **2**(1), 403 (2011).
37. L. Yang, T. Carmon, B. Min, *et al.*, "Erbium-doped and Raman microlasers on a silicon chip fabricated by the sol–gel process," Appl. Phys. Lett. **86**(9), 091114 (2005).
38. A. A. Savchenkov, A. B. Matsko, and L. Maleki, "White-light whispering gallery mode resonators," Opt. Lett. **31**(1), 92–94 (2006).